Journal of Neuroimaging in Psychiatry & Neurology

https://doi.org/10.17756/jnpn.2021-038

Research Article

Open Access

Convolutional Neural Networks Accurately Predict Benign versus Malignant Status Among Peripheral Nerve Sheath Tumors

Alexander Mazal[1], Liyuan Chen[2], Feng Poh[3], Jing Wang[2], Michael Folkert[2], Oganes Ashikyan[4], Parham Pezeshk[4] and Avneesh Chhabra[4*]

[1]Department of Surgery and Perioperative Care, The University of Texas at Austin Dell Medical School, Austin, TX, USA
[2]Department of Radiation Oncology, UT Southwestern Medical Center, Dallas, Texas, USA
[3]Mount Elizabeth Hospital, Singapore
[4]Division of Musculoskeletal Radiology, Department of Radiology, UT Southwestern Medical Center, Dallas, TX, USA

[*]Correspondence to:
Avneesh Chhabra, MD
Associate Professor of Radiology
Chief, Division of Musculoskeletal Radiology
UT Southwestern Medical Center
Harry Hines Blvd, Dallas, TX, USA
E-mail: Avneesh.Chhabra@UTSouthwestern.edu

Received: January 11, 2021
Accepted: February 19, 2021
Published: February 22, 2021

Citation: Mazal A, Chen L, Poh F, Wang J, Ashikyan O, et al. 2021. Convolutional Neural Networks Accurately Predict Benign versus Malignant Status Among Peripheral Nerve Sheath Tumors. *J Neuroimaging Psychiatry Neurol* 6(1): 1-6.

Published by United Scientific Group

Abstract

Background: Peripheral nerve sheath tumors (PNSTs) comprise ~5-10% of soft tissue tumors encountered in the clinical setting. Benign lesions (BPNSTs), such as neurofibromas and schwannomas are often asymptomatic or cause neuropathy. Malignant peripheral nerve sheath tumors (MPNSTs) frequently exhibit rapid invasive behavior and metastatic spread. MR imaging markers do not reliably differentiate BPNSTs from MPNSTs. Convolutional neural networks employ machine learning and multi-order statistics to derive imaging signatures that could improve diagnostic assessment of PNSTs.

Purpose: To evaluate whether convolutional neural networks can accurately differentiate BPNSTs from MPNSTs and compare the accuracy to that of expert radiologist interpretation.

Materials and Methods: MR images from 47 patients with histologically-confirmed PNSTs were identified. Two separate convolutional neural networks (CNNs) were created using fat-suppressed T2-weighted (fsT2W) images alone (CNN 1), and fsT2W images in combination with pre- and post-contrast T1-weighted imaging (CNN 2). CNN performance was compared to interpretation by two experienced radiologists.

Results: CNN 1 performed comparably to the radiologists, achieving an accuracy and area under the curve (AUC) of 87% and 0.89, respectively. By comparison, radiologist 1 and 2 achieved accuracies and AUCs of 73%, 0.83 and 93%, 0.83, respectively. No significant differences were found between the accuracies or AUCs of either radiologist and CNN 1 ($p>0.05$). CNN 2 achieved an accuracy and AUC of 93%, 0.94. Using all image sequences together, radiologists 1 and 2 achieved accuracies and AUCs of 71%, 0.81 and 71%, 0.70, respectively.

Conclusion: Convolutional neural networks accurately differentiated BPNSTs versus MPNSTs in our investigation. Larger studies may be needed to validate these results.

Keywords

Radiomic analysis, Machine learning, Convolutional neural network, Peripheral nerve sheath tumor, Neurofibroma, Schwannoma, Malignant peripheral nerve sheath tumor

Introduction

PNSTs are a group of soft tissue neoplasms of Schwann cell and/or perineurial cell origin. They are broadly classified into benign PNSTs (BPNSTs) and malignant PNSTs (MPNSTs) based on their pathologic findings and clinical invasive behavior. Among BPNSTs, the most commonly observed subtypes are neurofibromas, schwannomas, and, more rarely, perineuriomas. BPNSTs may manifest clinically with neuropathy or compressive symptoms due to local growth and invasion, or they may remain asymptomatic. Neurofibromas, in particular, typically have fascicles of origin which are non-functional [1]. By comparison, MPNSTs exhibit rapid growth with early metastatic spread [2]. They are associated with significant morbidity and mortality and confer a bleak prognosis. Early identification and treatment of MPNSTs is essential for the prevention of serious sequelae [3]. MR imaging represents the gold standard for initial identification and differentiation of these neoplasms; however, there can often be considerable overlap in the imaging features of benign and malignant tumors (Figure 1). For this reason, conventional reader-based diagnostic approaches do not reliably differentiate "indeterminate" lesions, and a biopsy is required for definitive pathologic diagnosis. Due to the high prevalence of BPNSTs with borderline features concerning for malignancy, many patients with these lesions are unnecessarily referred for biopsy rather than follow-up [4]. Although adjuncts to conventional MR imaging have been purported to increase the diagnostic yield of initial imaging, including FDG18-PET imaging, diffusion-weighted imaging

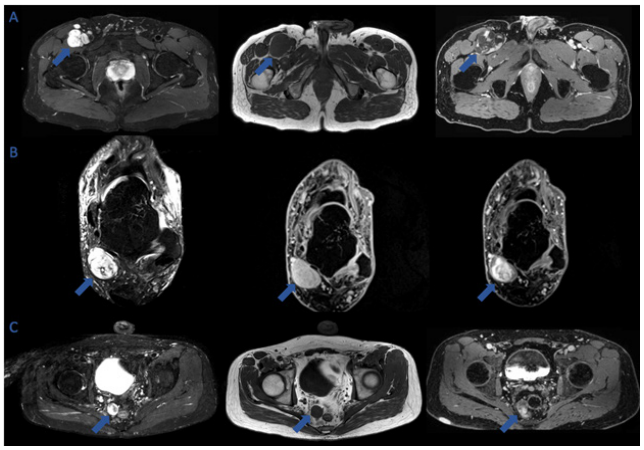

Figure 1: Benign and Malignant Peripheral Nerve Sheath Tumors Exhibit Overlapping Characteristics on Imaging **A)** Left to Right: T2FS, pre- and -post-contrast T1W images, respectively, of a benign neurofibroma in the setting of neurofibromatosis. With a maximum dimension of ~5 cm and heterogeneous pattern of enhancement, the tumor exhibits characteristics mimicking those of a malignant lesion. **B)** Left to Right: T2FS, pre- and post-contrast T1W images, respectively, of a benign neurofibroma of the right ankle. Regions of heterogeneous enhancement pattern are again visualized. **C)** Left to Right: T2FS, pre- and post-contrast T1W images, respectively, of extra-axial MPNST of the pelvis. Note the small diameter and borderline imaging characteristics of the lesion.

(DWI) and diffusion tensor imaging (DTI), further work is needed to determine the efficacy of these techniques [5]. In a 2014 study by Demehri et al., more than 1/3 of PNSTs with both conventional and functional imaging features that were reported as being highly concerning for malignancy (avg. size ≥4.2 cm and apparent diffusion coefficient (ADC) value <1.0 x 10-3 mm2/s), were in-fact benign [4]. More robust diagnostic imaging techniques are therefore currently being explored to improve diagnostic accuracy.

Radiomics is an emerging field, which represents the convergence of several disciplines, including radiology, machine learning, and computer vision [6]. Radiomic analysis relies on automated quantitative image analytics and the extraction of quantitative image features (referred to henceforth as radiomic features), which can be leveraged to improve medical decision making. Radiomic features such as shape, volume, texture (gray level co-occurrence matrix, intensity (i.e., first order statistics, or wavelet, among others) can offer insight into tumor phenotypic characteristics [7].

There has been considerable progress in the field of radiomics and convolutional neural networks (CNNs) over the past decade, with many studies demonstrating the potential utility of these techniques in tumor prognostication, staging, screening, survival, and recurrence risk [7-15]. Nevertheless, data concerning the utility of CNNs and radiomics in the domain of PNSTs remain sparse. This study evaluated the accuracy of convolutional neural networks in the differentiation of histologically proven benign and malignant PNSTs and compared it to that of expert radiologist interpretation. We hypothesized that trained CNN models would outperform the expert radiologist interpretations.

Methods

The study was conducted under institutional review board approval and the informed consent was waived.

Study population

MR images from 47 consecutive cases of PNSTs were gathered retrospectively from the institutional electronic medical record system (EMR) (dates 2006-2018), comprised of 36 benign and 11 malignant tumors, in total. Inclusion criteria were as follows: adult age (18-75 years), histologic confirmation of lesion, and lesions with MRI protocol containing sequences chosen to be analyzed (i.e. fsT2W and T1 pre- and post-contrast images). Exclusion criteria were as follows: incomplete imaging, presence of artifacts limiting evaluation of the lesions, central nervous system location, and pediatric age group. Patient and tumor characteristics are described in Table 1.

Imaging protocol parameters

Imaging protocol parameters were as follows: **A**) T1W images: Repetition time (TR) / Echo Time (TE) of 600-715 / 9-17 ms, 4 mm slice thickness, with axial and sagittal planes. **B**) fsT2W images: TR/TE of 3600-6000 / 60-62 ms, 4 mm slice thickness, in axial, coronal, and sagittal planes. **C**) Unenhanced and gadolinium enhanced-3-dimensional (3D) fsT1W modified Dixon: TR/TE of 4.6-6.3 / 1.4-1.5, 1.5 mm voxel thickness, in the coronal plane with isotropic

Table 1: Characteristics of patients and tumors.

	All Tumors	BPNSTs	MPNSTs
No. of patients	47	36	11
Age (years)	Mean: 41.5 Range: 19-75	Mean: 41.25 Range: 19-73	Mean: 42.4 Range: 21-75
Gender (male/ female)	Male: 17 Female: 30	Male: 11 Female: 25	Male: 6 Female: 5
Tumor characteristics	Enhancement pattern: Heterogeneous: 25 Homogeneous: 17 (5 tumors without contrast studies)	Enhancement pattern: Heterogeneous: 16 Homogeneous: 16 (4 tumors without contrast studies) Percent neurofibroma heterogeneously enhancing: 41% (9/22 tumors with contrast studies) Percent schwannoma heterogeneously enhancing: 70% (7/10 tumors with contrast studies)	Enhancement pattern: Heterogeneous: 9 Homogeneous: 1 (1 tumor without contrast study) Percent MPNST heterogeneously enhancing: 90% (9/10 tumors with contrast studies)
Size (max dimension)	Mean: 6.2 cm Range: 0.6 - 25 cm	Mean: 5.6 cm Range: 0.6 - 25 cm	Mean: 8.1 cm Range: 3.1 - 15.9 cm
Location:			
Limb	19	17	2
Torso	15	9	6
Head & Neck	13	10	3
Histology:			
Neurofibroma	23	23	
Schwannoma	13	13	
MPNST	11		11

axial and sagittal reconstructions. Contrast administered was intravenous gadolinium at the rate of 0.1 mmol/kg.

Image pre-processing

In each tumor, 3D volumes of interest (VOIs) corresponding to tumor boundaries **(**Figure 2**)** were manually segmented and contoured by a separate musculoskeletal radiologist (fellowship trained with 4 years of experience) using Velocity software (Varian Medical Systems).

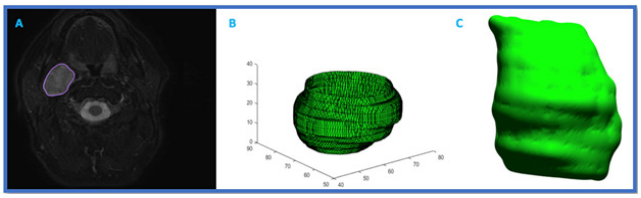

Figure 2: 3D segmentation of peripheral nerve sheath tumor 3D segmentation of peripheral nerve sheath tumor **A)** T2FS image of schwannoma in right submandibular region. Purple ellipse represents contour of manually segmented tumor boundaries. **B)** 3D computer reconstruction of tumor volume after tumor segmentation. Axis measurements are in millimeters. **C)** 3D computer reconstruction visualizing tumor surface features.

Model development, validation, and testing

For system training and validation of CNN 1, data extracted from VOIs of fsT2W images of 25 tumors (17 benign, 8 malignant) were used for the proposed CNN, which included 7 convolutional, 3 max-pooling, and 2 fully connected layers (Figure 3). Data augmentation by rotating 3D images and synthetic minority oversampling technique (SMOTE) were employed to balance and increase training samples. CNN model 2 consists of three separate CNN models (same architecture with that of CNN 1) with each trained and validated by VOIs from fsT2W, T1 pre- or post-contrast images of 17 tumors (14 benign, 3 malignant). Data augmentation and SMOTE techniques were employed as well. Each CNN model would generate a predictive malignancy probability for each tumor. Evidential reasoning

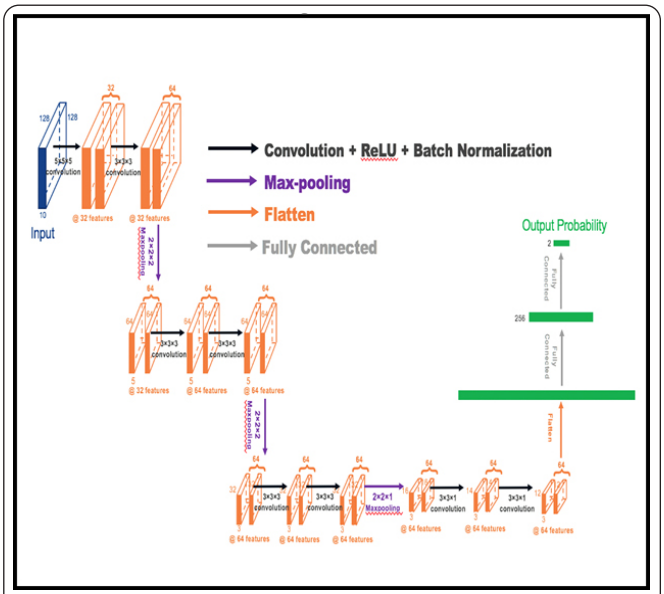

Figure 3: Convolutional neural network architecture. Convolutional neural network featuring 7 convolutional, 3 max-pooling, and 2 fully-connected layers.

(ER) fusion algorithm was utilized to fuse the probabilities obtained by these three separate models to generate a final predictive result for CNN 2. System training and testing were performed by a post-doctoral research fellow specializing in artificial intelligence techniques.

For testing of the CNN models and radiologists, a group of unknown tumors was collected into two testing datasets: one test set of 15 unknown tumors with only fsT2W images, and one test set of 14 tumors with all imaging data (fsT2W + T1 pre- and post-contrast). Because only 14 tumors of the testing sample had associated T1 pre-contrast imaging, for the final testing results, 14 tumors (as opposed to 15) were considered for testing of CNN 2. The accuracies of the CNN models were evaluated using the corresponding test datasets.

The same test datasets were administered to two other experienced musculoskeletal radiologists (with MSK fellowship training and 4 and 8 years of experience, respectively). Clinical background data or histology results were not made available to the radiologists.

Statistics

Statistical tests included area under the curve (AUC) and Fisher's Exact Test for comparison of accuracy between the CNN models and radiologists. A paired empirical (nonparametric) ROC curve analysis was performed using a contrast matrix to evaluate for differences in empirical ROC curves between CNN models and radiologists (in accordance with the method previously described by DeLong et al.) [16]. A p-value of $p<0.05$ was considered significant in all statistical analyses performed herein. Statistical analyses were performed by an expert statistician with experience in artificial intelligence techniques.

Results

A total of 47 tumors were utilized in this study, comprised of 36 benign and 11 malignant tumors (Table 1). Among benign tumors, 50% of lesions exhibited heterogeneous enhancement on post-contrast T1W imaging, versus 90% among MPNSTs. Tumors exhibited a wide range of dimensions among both benign and malignant lesions, with maximum dimensions ranging from 0.6 – 25 cm among the benign lesions and 3.1 cm – 15.9 cm among the MPNSTs, respectively.

The CNN 1 model predicted benign versus malignant status among PNSTs with an accuracy and AUC of 87%, 0.89, respectively (Table 2, Figure 4). By comparison, blinded radiologists with access to the same fsT2W imaging dataset achieved the following accuracies and AUCs: 73%, 0.83 for Radiologist 1, and 93%, 0.83 for Radiologist 2, respectively. No significant differences were found between the accuracies of CNN 1 and Radiologist 1 ($p>0.05$), CNN 1 and Radiologist 2 ($p>0.05$), or between Radiologists 1 and 2 ($p>0.05$) (Table 3). Similarly, no significant differences were found between the AUCs of CNN 1 and Radiologist 1 ($p>0.05$), CNN 1 and Radiologist 2 ($p>0.05$), or Radiologists 1 and 2 ($p>0.05$) (Table 4).

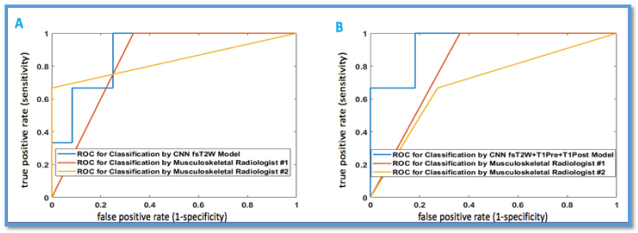

Figure 4: ROC curves for CNN models and radiologists. A) ROC curves of CNN 1, Radiologists 1 and 2 with access only to fsT2W testing images. B) ROC curves of CNN 2, Radiologists 1 and 2 with access to fsT2W, pre- and post-contrast T1W testing images.

Table 2: Accuracies and AUCs of CNN models and radiologists.

	Accuracy	AUC
CNN 1 (fsT2W)	87%	0.89
Radiologist 1	73%	0.83
Radiologist 2	93%	0.83
CNN 2 (fsT2W + T1W pre- and post-contrast)	93%	0.94
Radiologist 1	71%	0.81
Radiologist 2	71%	0.70

Both CNN models accurately classified benign versus malignant PNSTs. Note the apparent but insignificant drop in Radiologist performance when provided additional imaging data as compared to only T2FS.

Table 3: Difference in accuracies between CNN Models and radiologists.

Comparison Matrix	p-value (Fisher exact test statistic)
Radiologist 1: fsT2W vs All imaging	1
Radiologist 2: fsT2W vs All imaging	0.1686
Radiologist 1 vs Radiologist 2: fsT2W	0.3295
Radiologist 1 vs Radiologist 2: All imaging	1
Radiologist 1 vs CNN 1: fsT2W	0.6513
Radiologist 1 vs CNN 2: All imaging	0.3295
Radiologist 2 vs CNN 1: fsT2W	1
Radiologist 2 vs CNN 2: All imaging	0.3259
CNN 1 vs CNN 2	1

No significant differences were found between accuracies of CNN models and radiologists.

The CNN 2 model predicted benign versus malignant status among PNSTs with an accuracy and AUC of 93%, 0.94, respectively. Blinded radiologists with access to the same imaging dataset (including all imaging data from fsT2W, pre- and post-contrast T1W images mirroring the routine setting) achieved the following accuracies and AUCs: 71%, 0.81 for Radiologist 1, and 71%, 0.70 for Radiologist 2, respectively. No significant differences were found between the accuracies of CNN 2 and Radiologist 1 ($p>0.05$), CNN 2 and Radiologist 2 ($p>0.05$), or between Radiologists 1 and 2 ($p>0.05$). No significant differences were found between the AUCs of CNN 2 and Radiologist 1 ($p>0.05$), CNN 2 and Radiologist 2 ($p>0.05$), or Radiologists 1 and 2 ($p>0.05$).

Table 4: ROC contrast estimation between CNN models and radiologists.

Contrast Matrix	p-value
Radiologist 1: fsT2W vs All imaging	0.3173
Radiologist 2: fsT2W vs All imaging	0.0528
Radiologist 1 vs Radiologist 2: fsT2W	0.867
Radiologist 1 vs Radiologist 2: All imaging	0.5133
Radiologist 1 vs CNN 1: fsT2W	0.9131
Radiologist 1 vs CNN 2: All imaging	0.232
Radiologist 2 vs CNN 1: fsT2W	0.6961
Radiologist 2 vs CNN 2: All imaging	0.3504
CNN 1 vs CNN 2	0.232

Contrast estimation matrix comparing performance of CNN models and radiologists. No significant differences were observed.

When comparing the AUCs of Radiologist 1 with access only to fsT2W images versus all imaging data, no significant difference between AUCs was observed (p>0.05). Likewise, in a comparison between the AUCs of Radiologist 2 with access only to fsT2W images versus all imaging data, no significant difference between AUCs was observed, however, this value fell, just short of significance (p=0.0528).

Discussion

In the comparison of diagnostic performance between the two CNN models and blinded expert radiologists, the CNN models performed comparably or exceeded reader performance in the differentiation of BPNSTs and MPNSTs. The p-values did not reach significance, which may be related to the small sample size. Using fsT2W images in isolation, the accuracies of both CNN 1 and CNN 2 models did not vary significantly from those of either Radiologist 1 or 2 (p>0.05). Interestingly, there was an apparent fall in performance among both radiologists with access to all imaging data, and their performance appeared to be better using only fsT2W images. This could possibly be attributed to the heterogeneous enhancement patterns observed in some benign tumors. Such tumor characteristics are well-described and are not uncommon in the clinical setting, leading to diagnostic dilemmas [4, 17-19]. Heterogeneous enhancement and intra-tumoral necrosis are particularly common findings among ancient schwannomas; however, they can also be seen sometimes in the setting of other BPNSTs such as plexiform neurofibromas [19]. Within this study, 70% of benign schwannomas and 41% of neurofibromas exhibited heterogeneous enhancement. Larger dimensions (ranging up to 25 cm) were also commonly observed among benign lesions, particularly among patients with neurofibromatosis Type I (NF-1). Likewise, these features are commonly observed with MPNSTs. MPNSTs have been reported to differ from BPNSTs by their larger diameter (> 5 cm), peri-lesional edema, peripheral or heterogeneous enhancement, and intra-tumoral necrosis or hemorrhage [20]. Although in combination, these features confer a high specificity for malignancy, such features are insensitive and are not present in all MPNSTs [20]. Given the presence of many of these features in benign tumors, CNNs may serve as a particularly useful diagnostic tool with PNSTs demonstrating borderline or intermediately concerning imaging characteristics. It may also help reduce the number of unnecessary biopsies among patients with NF-1, in whom larger benign lesions with inhomogeneous enhancement are particularly common.

The study was limited by a small sample size, as only histology-proven diagnoses were included; however, study subjects were identified randomly and are believed to represent a sufficiently representative sample to render these results generalizable and reproducible for other medical centers. Future studies with larger testing datasets will be essential to increase the power sufficiently to discern more subtle differences in performance between CNN models and expert readers. Furthermore, due to the presence of imbalanced classes within the testing datasets, which heavily favored representation of benign lesions, there were additional limitations on the statistical inferences which could be drawn herein. The presence of a minority class (MPNSTs) in the dataset predisposes to misclassification and is inappropriate in the setting of machine learning algorithms set to evaluate accuracy, as it may yield poor predictive accuracy in the minority class. To reconcile this imbalance, SMOTE was utilized to oversample the minority class and balance the dataset, with good resulting accuracy and AUC, as observed by both CNN models.

Because CNN models were utilized in this study, we did not seek to extract specific radiomic features. Future studies with larger cohorts may help further delineate individual clinical biomarkers indicative of malignancy. Further studies will also be necessary to determine whether CNNs or radiomics can play a role in the differentiation of BPNST subtypes, which was not pursued herein.

Finally, an additional limitation of this study was that radiologists were not given access to clinical history or other supplementary data that would ordinarily be found in the routine setting, as we sought to specifically compare unbiased reader performance to the machine reads.

Conclusion

In conclusion, the results of this study demonstrate that CNNs differentiate benign and malignant PNSTs with high accuracy, particularly using multiple imaging sequences in combination modeling the routine setting. In future clinical practice, CNNs are most likely to serve as a useful tool in differentiating PNSTs with borderline imaging features concerning for malignancy

References

1. Levi AD, Ross AL, Cuartas E, Qadir R, Temple HT. 2010. The surgical management of symptomatic peripheral nerve sheath tumors. *Neurosurgery* 66(4): 833-840. https://doi.org/10.1227/01.NEU.0000367636.91555.70

2. Farid M, Demicco EG, Garcia R, Ahn L, Merola PR, et al. 2014. Malignant peripheral nerve sheath tumors. *Oncologist* 9(2): 193-201. https://doi.org/10.1634/theoncologist.2013-0328

3. Kim DH, Murovic JA, Tiel RL, Moes G, Kline DG. 2005. A series of 397 peripheral nerve sheath tumors: 30-year experience at Louisiana State University Health Science Center. *J Neurosurg* 102(2): 246-255. https://doi.org/10.3171/jns.2005.102.2.0246

4. Demehri S, Belzberg A, Blakeley J, Fayad LM. 2014. Conventional and functional MR imaging of peripheral nerve sheath tumors: initial experience. *AJNR Am J Neuroradiol* 35(8): 1615-1620. https://doi.org/10.3174/ajnr.A3910

5. Shahid KR, Amrami KK, Esther RJ, Lowe VJ, Spinner RJ. 2011. False-negative fluorine-18-fluorodeoxyglucose positron emission tomography of a malignant peripheral nerve sheath tumor arising from a plexiform neurofibroma in the setting of neurofibromatosis type 1. *J Surg Orthop Adv* 20(2): 132-135

6. Zhou M, Scott J, Chaudhury B, Hall L, Goldgof D, et al. 2018. Radiomics in brain tumor: image assessment, quantitative feature descriptors, and machine-learning approaches. *AJNR Am J Neuroradiol* 39(2): 208-216. https://doi.org/10.3174/ajnr.A5391

7. Lambin P, Leijenaar RTH, Deist TM, Peerlings J, de Jong EEC, et al. 2017. Radiomics: the bridge between medical imaging and personalized medicine. *Nat Rev Clin Oncol* 14(12): 742-762. https://doi.org/10.1038/nrclinonc.2017.141

8. Aerts H, Velazquez ER, Leijenaar RTH, Parmar C, Grossmann P, et al. 2014. Decoding tumor phenotype by noninvasive imaging using a quantitative radiomics approach. *Nat Commun* 5: 4006. https://doi.org/10.1038/ncomms5006

9. van Rossum PS, Fried DV, Zhang L, Hofstetter WL, van Vulpen M, et al. 2016. The incremental value of subjective and quantitative assessment of 18F-FDG PET for the prediction of pathologic complete response to preoperative chemoradiotherapy in esophageal cancer. *J Nucl Med* 57(5): 691-700. https://doi.org/10.2967/jnumed.115.163766

10. Coroller TP, Grossman P, Hou Y, Velazquez ER, Leijenaaret RTH al. 2015. CT-based radiomic signatures predict distant metastasis in lung adenocarcinoma. *Radiother Oncol* 114(3): 345-50. https://doi.org/10.1016/j.radonc.2015.02.015

11. Liang C, Huang Y, He L, Chen X, Ma Zelan, et al. 2016.The development and validation of a CT-based radiomics signature for the preoperative discrimination of stage I-II and stage II-IV colorectal cancer. *Oncotarget* 7(21): 31401-3112. https://doi.org/10.18632/oncotarget.8919

12. Hawkins S, Wang H, Liu Y, Garcia A, Stringfield O, et al. 2016. Predicting Malignant Nodules from Screening CT Scans. *J Thorac Oncol* 11(12): 2120-2128. https://doi.org/10.1016/j.jtho.2016.07.002

13. Grossman P, Gutman DA, Dunn WD Jr., Holder CA, Aerts HJWL, et al. 2016. Imaging-genomics reveals driving pathways of MRI derived volumetric tumor phenotype features in Glioblastoma. *BMC Cancer* 16: 611. https://doi.org/10.1186/s12885-016-2659-5

14. Huang Y, Liu Z, He L, et al. 2016. Radiomics signature: a potential biomarker for the prediction of disease-free survival in early-stage (I or II) non-small cell lung cancer. *Radiology* 281(3): 947-957. https://doi.org/10.1148/radiol.2016152234

15. Li H, Zhu Y, Burnside ES, Drukker D, Hoadley KA, et al. 2016. MR imaging radiomics signatures for predicting the risk of breast cancer recurrence as given by research versions of mammaprint, oncotype DX, and PAM50 gene assays. *Radiology* 281(2): 382-391. https://doi.org/10.1148/radiol.2016152110

16. DeLong ER, DeLong DM, Clarke-Pearson DL. 1988. Comparing the areas under two or more correlated receiver operating characteristic curves: a nonparametric approach. *Biometrics* 44(3): 837-45

17. Hanemann CO, Evans DG. 2006. News on the genetics, epidemiology, medical care and translational research of Schwannomas. *J Neuro1* 253(12): 1533-1541. https://doi.org/10.1007/s00415-006-0347-0

18. Mazal AT, Ashikyan O, Cheng J, et al. 2018. Diffusion-weighted imaging and diffusion tensor imaging as adjuncts to conventional MRI for the diagnosis and management of peripheral nerve sheath tumors: current perspectives and future directions. *Eur Radiol* 29(8): 4123-4132. https://doi.org/10.1007/s00330-018-5838-8

19. Ahlawat S, Blakeley J, Montgomery E, Subramaniam RM, Belzberg A, et al. 2013. Schwannoma in neurofibromatosis type 1: a pitfall for detecting malignancy by metabolic imaging. *Skeletal Radiol* 42(9): 1317-1322. https://doi.org/10.1007/s00256-013-1626-3

20. Wasa J, Nishida, Tsukushi S, Shido Y, Sugiura H, et al. 2010. MRI features in the differentiation of malignant peripheral nerve sheath tumors and neurofibromas. *AJR Am J Roentgenol* 194(6): 1568-1574. https://doi.org/10.2214/AJR.09.2724